

Galaxies with Supermassive Binary Black Holes: (III) The Roche Lobes and Jiang-Yeh Lobe in a Core System

Li-Chin Yeh¹ and Ing-Guey Jiang²

¹*Department of Applied Mathematics,
National Hsinchu University of Education, Hsin-Chu, Taiwan*

²*Department of Physics and Institute of Astronomy,
National Tsing-Hua University, Hsin-Chu, Taiwan*

jiang@phys.nthu.edu.tw

ABSTRACT

Three-dimensional equi-potential surfaces of a galactic system with supermassive binary black holes are discussed herein. The conditions of topological transitions for the important surfaces, i.e. Roche Lobes and Jiang-Yeh Lobe, are studied in this paper. In addition, the mathematical properties of the Jacobi surfaces are investigated analytically. Finally, a numerical procedure for determining the regions of the Roche Lobes and Jiang-Yeh Lobe is suggested.

1. Introduction

It is known that most galaxies, if not all, host supermassive black holes, as implied by the stellar kinematic data and the radiation of active galactic nuclei near the centers of galaxies. Among these, early-type galaxies were likely constructed through the merging events of spiral galaxies. Therefore, they might host more than one supermassive black holes. The evolution of these supermassive black holes shall be related to the merging processes and the properties of those involved galaxies. Supermassive black holes will then scatter their surrounding stars and therefore influence the structures of galaxies as feedback. In fact, the possible co-evolution of galaxies and supermassive black holes has become one of the most important and popular astronomical topics in recent years.

In a merged galactic system, supermassive black holes will be driven to the galactic center by dynamical friction. When there is more than one supermassive black holes, i.e. two or three, it is likely that supermassive binary black holes (SBBH) will form in the galactic center. A configuration of three or more such bodies is less stable due to possible dynamical instabilities among three or multiple bodies. In order to study the evolution of

SBBH, Quinlan (1996) carried out numerical experiments on the stellar scattering by SBBH in the form of restricted three-body problems. Indeed, the restricted three-body problem has been a useful model in many fields, such as the evolution of binary stars (Eggleton 1983) and orbital calculations of planetary systems (Mikkola et al. 1994; Namouni 1999). Moreover, modifications of the restricted three-body problem were employed to model various problems related to planetary systems (Chermnykh 1987; Papadakis 2004, 2005a, 2005b; Jiang & Yeh 2006; Yeh & Jiang 2006; Perdios, Kalantonis & Douskos 2008; Kushvah 2008a, 2008b, 2009, 2011a, 2011b; Douskos 2011; Kushvah, Kishor & Dolas 2012; Kishor & Kushvah 2013; Douskos et al. 2012; Douskos 2015).

On the other hand, n-body simulations also play important roles in the study of galactic mergers (Wu & Jiang 2009, 2012, 2015). Milosavljevic & Merritt (2001) employed n-body simulations to study the orbital decay of black holes and the formation of SBBHs during galactic mergers. Once an SBBH is formed at the galactic center, it is important to understand how it affects the central surface brightness of a galaxy. If that can be done, the relationship between the surface brightness profiles and properties of SBBH might be established.

Motivated by that goal of establishing SBBH–brightness connections, Jiang & Yeh (2014a) took a first step to construct a theoretical model with an SBBH embedded in a galactic center. Their employed galactic density profile was the same as one of those suggested in Kandrup et al. (2003), i.e.:

$$\rho(\bar{r}) = \rho_c \left(\frac{\bar{r}}{r_b} \right)^{-\gamma} \left\{ 1 + \left(\frac{\bar{r}}{r_b} \right)^\alpha \right\}^{\frac{\gamma-\beta}{\alpha}}, \quad (1)$$

where ρ_c , r_b , α , β and γ are the constants. In fact, these density profiles are equivalent to the (α, β, γ) -models in Hernquist (1990), albeit with different parameter definitions; it is a five-parameter generalization of Jaffe’s double-power law model. Zhao (1996) found that the gravitational potentials corresponding to these density profiles could have simple analytic forms for certain choices of α , β and γ . Jiang & Yeh (2014a) investigated the existence of equilibrium points, i.e. Lagrange Points and Jiang-Yeh Points, for a system with $\alpha = 2$, $\beta = 4$ and $\gamma = 0$, i.e. a core density profile. They proved that Jiang-Yeh Points exist if, and only if, the galactic mass is larger than a critical mass. Moreover, Jiang & Yeh (2014b) found that Jiang-Yeh Points always exist for a system with $\alpha = 2$, $\beta = 5$ and $\gamma = 1$, i.e. a cuspy density profile.

In these models, the orbital motion of stars near the SBBH at the centers of galaxies can be determined conveniently as a modification of restricted three-body systems. Because the time-scales of the SBBH orbital changes and the variations of overall galactic potential are much larger than the dynamical time near the galactic center, the stellar orbits derived

from these models are good approximations of realistic n-body simulations. The surface brightness of galactic centers can be calculated when stellar orbits have been obtained. The surface brightness near the center of galaxies might show some signals which are related to the dynamical evolution of stars near the SBBH. Therefore, these models can become useful tools for interpreting the properties of SBBH from the observational surface brightness of galaxies.

For such an SBBH model, it would be interesting to understand precisely how stars move around supermassive black holes. It is important to investigate whether stars would stay within an equi-potential surface centered on one supermassive black hole, or jump to another one under particular conditions. For the above purpose, we will present the shape and topology of equi-potential surfaces, and be able to determine whether stars are inside or outside one of equi-potential surfaces in three dimensional space.

Thus, the main goal of this paper is to extend the model in Jiang & Yeh (2014a) into a three-dimension model and present the equi-potential surface. The condition under which the important surfaces would have topological changes will also be investigated.

Moreover, we will also analytically study the properties of the Jacobi integral of equi-potential surfaces, and suggest a numerical procedure to determine the regions of important equi-potential surfaces.

The model is given in Section 2, the equi-potential surfaces are presented in Section 3, the mathematical properties of the Jacobi surfaces are studied in Section 4, the determination of regions of Roche Lobes and Jiang-Yeh Lobe is in Section 5, and the concluding remarks are presented in Section 6.

2. The Model

The dynamics of a star near the center of a galaxy in a three-dimensional space is studied herein. The star is governed by the galactic potential and the gravitational force from the central SBBH. As in Jiang & Yeh (2014a), the star is treated as a test particle, the galactic potential is fixed, and the SBBH is an equal-mass pair moving along a circular orbit. The galactic density distribution could have any form as long as it is spherically symmetric. A power law with a core, as the profile used in Jiang & Yeh (2014a), is adopted herein:

$$\rho(\bar{r}) = \rho_c \left\{ 1 + \left(\frac{\bar{r}}{r_b} \right)^2 \right\}^{-2}, \quad (2)$$

where ρ_c is a constant. The scale length r_b is called the break radius. When $\bar{r} \gg r_b$, the above becomes a power law with index 4. For $\bar{r} \ll r_b$, the density approaches becoming a constant as \bar{r} gets close to zero. Thus, the break radius, r_b , marks a transition from the outer power law with index 4 to the core of the system. It is also called the core radius here. The mass of the galaxy up to a radius \bar{r} is expressed as :

$$M(\bar{r}) = 4\pi \int_0^{\bar{r}} r_{du}^2 \rho(r_{du}) dr_{du} = 2\pi\rho_c \left\{ \tan^{-1}(\bar{r}/r_b) - \frac{(\bar{r}/r_b)}{1 + (\bar{r}/r_b)^2} \right\}, \quad (3)$$

where r_{du} is a dummy variable of the integration. Note that the galactic mass $M(\bar{r})$ does not include the mass of SBBH. The galactic total mass is set to be M_g ; thus the constant $\rho_c = M_g\pi^{-2}$.

Moreover, the corresponding potential is expressed as:

$$V(\bar{r}) = -4\pi \left[\frac{1}{\bar{r}} \int_0^{\bar{r}} \rho(r_{du}) r_{du}^2 dr_{du} + \int_{\bar{r}}^{\infty} \rho(r_{du}) r_{du} dr_{du} \right] = -c \frac{\tan^{-1}(\bar{r}/r_b)}{(\bar{r}/r_b)}, \quad (4)$$

where $c = 2M_g\pi^{-1}$. With this galactic potential and the SBBH at $(-\bar{R}, 0, 0)$, $(\bar{R}, 0, 0)$, the equations of motion of a star under the rotating frame in a three-dimensional space are now written as

$$\left\{ \begin{array}{l} \frac{d\bar{x}}{dt} = \bar{u} \\ \frac{d\bar{y}}{dt} = \bar{v} \\ \frac{d\bar{z}}{dt} = \bar{w} \\ \frac{d\bar{u}}{dt} = 2\bar{n}\bar{v} + \bar{n}^2\bar{x} - \frac{G\bar{m}(\bar{x}+\bar{R})}{\bar{r}_1^3} - \frac{G\bar{m}(\bar{x}-\bar{R})}{\bar{r}_2^3} - \frac{\partial V}{\partial \bar{r}} \frac{d\bar{r}}{d\bar{x}} \\ \frac{d\bar{v}}{dt} = -2\bar{n}\bar{u} + \bar{n}^2\bar{y} - \frac{G\bar{m}\bar{y}}{\bar{r}_1^3} - \frac{G\bar{m}\bar{y}}{\bar{r}_2^3} - \frac{\partial V}{\partial \bar{r}} \frac{d\bar{r}}{d\bar{y}} \\ \frac{d\bar{w}}{dt} = -\frac{G\bar{m}\bar{z}}{\bar{r}_1^3} - \frac{G\bar{m}\bar{z}}{\bar{r}_2^3} - \frac{\partial V}{\partial \bar{r}} \frac{d\bar{r}}{d\bar{z}}, \end{array} \right. \quad (5)$$

where \bar{n} is the SBBH's angular velocity,

$$\bar{r} = \sqrt{\bar{x}^2 + \bar{y}^2 + \bar{z}^2}, \bar{r}_1 = \sqrt{(\bar{x} + \bar{R})^2 + \bar{y}^2 + \bar{z}^2}, \quad \text{and} \quad \bar{r}_2 = \sqrt{(\bar{x} - \bar{R})^2 + \bar{y}^2 + \bar{z}^2}.$$

As in Yeh, Chen, & Jiang (2012) and Jiang & Yeh (2014a), we can employ non-dimensionalization to simplify the above equations. When non-dimensional variables are set as

$$x = \frac{\bar{x}}{L_0}, y = \frac{\bar{y}}{L_0}, z = \frac{\bar{z}}{L_0}, r = \frac{\bar{r}}{L_0}, R = \frac{\bar{R}}{L_0}, t = \frac{\bar{t}}{t_0}, m = \frac{\bar{m}}{m_0}, u = \frac{\bar{u}}{u_0}, v = \frac{\bar{v}}{u_0}, w = \frac{\bar{w}}{u_0}, n = t_0\bar{n},$$

and some of the above parameters are further assumed to satisfy $u_0 = \frac{L_0}{t_0}$, $Gm_0 = \frac{L_0^3}{t_0^2}$,

$L_0 = r_b$, System (5) can be rewritten as

$$\left\{ \begin{array}{l} \frac{dx}{dt} = u \\ \frac{dy}{dt} = v \\ \frac{dz}{dt} = w \\ \frac{du}{dt} = 2nv + n^2x - \frac{m(x+R)}{r_1^3} - \frac{m(x-R)}{r_2^3} + \frac{cx}{r} \left\{ \frac{1}{(1+r^2)r} - \frac{\tan^{-1}r}{r^2} \right\} \\ \frac{dv}{dt} = -2nu + n^2y - \frac{my}{r_1^3} - \frac{my}{r_2^3} + \frac{cy}{r} \left\{ \frac{1}{(1+r^2)r} - \frac{\tan^{-1}r}{r^2} \right\} \\ \frac{dw}{dt} = -\frac{mz}{r_1^3} - \frac{mz}{r_2^3} + \frac{cz}{r} \left\{ \frac{1}{(1+r^2)r} - \frac{\tan^{-1}r}{r^2} \right\}. \end{array} \right. \quad (6)$$

Moreover, in the above equations, under the influence of the galactic potential, the mean motion, i.e. angular velocity, of each component of SBBH satisfies

$$mn^2R = \frac{m^2}{(2R)^2} + m|f_g(R)|. \quad (7)$$

That is, the centrifugal force of a black hole is equal to the total of the forces from another black hole and the background galaxy. The gravitational force per unit mass at r from the galactic potential, i.e. $f_g(r)$, can be expressed as

$$f_g(r) = c \left\{ \frac{1}{(1+r^2)r} - \frac{\tan^{-1}r}{r^2} \right\}. \quad (8)$$

Therefore,

$$n = \left\{ \frac{m}{4R^3} + \frac{1}{R}|f_g(R)| \right\}^{1/2}. \quad (9)$$

The corresponding Jacobi integral of this system is

$$C_J = 2U - \dot{x}^2 - \dot{y}^2 - \dot{z}^2 = n^2(x^2 + y^2) + \frac{2m}{r_1} + \frac{2m}{r_2} + 2c \frac{\tan^{-1}(r)}{r} - \dot{x}^2 - \dot{y}^2 - \dot{z}^2, \quad (10)$$

where $r = \sqrt{x^2 + y^2 + z^2}$, $r_1 = \sqrt{(x+R)^2 + y^2 + z^2}$, and $r_2 = \sqrt{(x-R)^2 + y^2 + z^2}$.

3. Equi-Potential Surfaces: Roche Lobes and Jiang-Yeh Lobe

As shown in last section, we have extended our equations of motion from two-dimensional space (Jiang & Yeh 2014a) to three-dimensional space. Because the SBBH is moving on the xy -plane, all results about equilibrium points presented in Jiang & Yeh (2014a) are also valid here. Thus, Jiang-Yeh Points could exist and would influence the structures of equi-potential surfaces in the system. Those equi-potential surfaces cutting through equilibrium

points would have the shapes of lobes. Two lobes centering on black holes are still called Roche Lobes, and the new one cutting through the Jiang-Yeh Points are called Jiang-Yeh Lobe in this paper.

Roche Lobes of the standard restricted three-body problem are equi-potential surfaces cutting through the first Lagrange Point L1. Each lobe centers on one star and connects with another lobe through L1. On the rotating frame of this binary system, test particles are locally force-free along the directions which are tangential to the equi-potential surfaces. This is why the Roche-lobe-over-flow could accomplish the mass transfer from one star to another (see Fig. 1(a)).

The Jacobi integral in Eq. (10) contains the potential part and the kinetic part. Taking $\dot{x} = \dot{y} = \dot{z} = 0$ in Jacobi integral would lead to equi-potential surfaces (equivalently, zero-velocity surfaces). For convenience, this particular case of the Jacobi integral is set as

$$F(x, y, z) \equiv n^2(x^2 + y^2) + \frac{2m}{r_1} + \frac{2m}{r_2} + 2c \frac{\tan^{-1}(r)}{r}, \quad (11)$$

and $F(x, y, z)$ is called *the Jacobi surfaces* here. For a given value of J , $F(x, y, z) = J$ is an equi-potential surface. The equi-potential surface cutting through a particular equilibrium point can be easily determined. For example, the coordinate of a given equilibrium point (x_E, y_E, z_E) is inserted into $F(x, y, z)$, and we set the constant $F(x_E, y_E, z_E) \equiv J_E$. Thus, $F(x, y, z) = J_E$ is an equi-potential surface cutting through this equilibrium point. Moreover, $F(x, y, 0) = J_E$ defines an equi-potential curve (zero-velocity curve) on the xy -plane, and $F(x, 0, z) = J_E$ defines an equi-potential curve on the xz -plane.

The convention of the names of equilibrium points here is the same as in Jiang & Yeh (2014a). That is, the equilibrium point at the origin (0,0,0) is Lagrange Point 1 (L1), the one at x -axis with $x > R$ is Lagrange Point 2 (L2), the one at x -axis with $x < -R$ is Lagrange Point 3 (L3), the one at y -axis with $y > 0$ is Lagrange Point 4 (L4), the one at y -axis with $y < 0$ is Lagrange Point 5 (L5), the one at x -axis with $0 < x < R$ is Jiang-Yeh Point 1 (JY1), the one at x -axis with $-R < x < 0$ is Jiang-Yeh Point 2 (JY2).

In order to present these equi-potential surfaces and curves, Models A, B, C and D are chosen as four cases with different sets of parameters. The values of their parameters are listed in the top three rows of Table 1. The resulting plots are shown in Figs.1-4, respectively. Because we consider equal mass SBBH, the system is symmetric. All important points we define and mark in Figs. 1-4 are in the regions with non-negative x, y, z coordinates.

In Model A, our system's parameters are $M_g = 0$, $m = R = 1$. The L1-passing equi-potential surfaces, i.e. the Roche Lobes, are shown in Fig. 1(a). Both the L1-passing and L2-passing equi-potential curves on the xy -plane and xz -plane are presented in Figs.

1(b)-(c). On the yz -plane, the equi-potential curves with $x = R$, i.e. $F(R, y, z) = J_{L1}$ and $F(R, y, z) = J_{L2}$, are plotted in Fig. 1(d). From these plots, it is clear that two Roche Lobes are connected at L1, which is simply the same as in the classic binary models. In Figs. 1(b)-(c), the equi-potential curve $F(x, y, 0) = J_{L1}$ or $F(x, 0, z) = J_{L1}$ goes through x -axis at L1, $(0, 0, x_{L1})$, and another point which is set as $(x_a, 0, 0)$.

The intersection between the equi-potential curve $F(x, y, 0) = J_{L1}$ and the line $x = R$ is set as $(R, y_a, 0)$; the intersection between the equi-potential curve $F(x, y, 0) = J_{L2}$ and the line $x = R$ is set as $(R, y_b, 0)$; the intersection between the equi-potential curve $F(x, 0, z) = J_{L1}$ and the line $x = R$ is set as $(R, 0, z_a)$; the intersection between the equi-potential curve $F(x, 0, z) = J_{L2}$ and the line $x = R$ is set as $(R, 0, z_b)$.

In Model B, our system's parameters are set as $M_g = 10$, $m = R = 1$. The structures of the equi-potential surfaces and curves are presented in Fig. 2. From Figs. 2(b)-(c), we find that the L1-passing equi-potential curves are not closed, while the L2-passing equi-potential curves form closed loops. Thus, the L2-passing equi-potential surfaces in three dimensional space are defined as the Roche Lobes, as shown in Fig. 2(a). The equi-potential curves on the yz -plane with $x = R$, i.e. $F(R, y, z) = J_{L1}$ and $F(R, y, z) = J_{L2}$, are plotted in Fig. 2(d). In Figs. 2(b)-(c), the equi-potential curve $F(x, y, 0) = J_{L2}$ or $F(x, 0, z) = J_{L2}$ goes through x -axis at L2, $(0, 0, x_{L2})$, and another point which is set as $(x_b, 0, 0)$. The marked y_a , y_b , z_a and z_b were defined previously, as in Fig. 1.

In Model C, when our system's parameters are $M_g = 30$, $m = R = 1$, Jiang-Yeh Points, i.e. JY1 and JY2, exist. As shown in Figs. 3(b)-(c), the equi-potential curves which pass JY1 and JY2 form a central closed loop. The L2-passing equi-potential curves also form closed loops centered on black holes. The JY1-JY2-passing equi-potential surfaces in three dimensional space are defined as Jiang-Yeh Lobe, and the L2-passing equi-potential surfaces in three dimensional space are still defined as the Roche Lobes here, as presented in Fig. 3(a). The equi-potential curve on the yz -plane with $x = 0$, i.e. $F(0, y, z) = J_{JY1}$, is plotted in Fig. 3(d). The marked x_b , y_b and z_b were defined previously as in Figs. 2 and 1. The coordinate of JY1 is $(0, 0, x_{JY1})$. The intersection between $F(x, y, 0) = J_{JY1}$ and the line $x = R$ is set as $(R, y_c, 0)$; the intersection between $F(x, y, 0) = J_{JY1}$ and the line $x = 0$, i.e. y -axis, is set as $(0, y_d, 0)$. The intersection between $F(x, 0, z) = J_{JY1}$ and the line $x = R$ is set as $(R, 0, z_c)$; the intersection between $F(x, 0, z) = J_{JY1}$ and the line $x = 0$ is set as $(0, 0, z_d)$.

In Model D, when the parameters are set as $M_g = 30$, $m = 1$, $R = 2$, Jiang-Yeh Points also exist. In Figs. 4(b)-(c), the JY1-JY2-passing equi-potential curves form three connected closed loops. Thus, in three dimensional space, the JY1-JY2-passing equal potential surfaces form three lobes, as presented in Fig. 4(a). The central one is defined as the Jiang-Yeh

Lobe, and the outer two are the Roche Lobes. The equi-potential curve $F(x, y, 0) = J_{JY1}$ or $F(x, 0, z) = J_{JY1}$ goes through x -axis at JY1 and another point which is set as $(x_c, 0, 0)$. The marked y_b, y_c, y_d, z_b, z_c and z_d were defined previously. The equi-potential curves on the yz -plane with $x = 0$, i.e. $F(0, y, z) = J_{L1}$ and $F(0, y, z) = J_{L2}$, are plotted in Fig. 4(d).

Apparently, the existence of galactic mass M_g changes the system's dynamical structure and separates two Roche Lobes. When $m = R = 1$ and M_g is between 0 and 10, i.e. Models A and B, there are no Jiang-Yeh Points, but the Roche Lobes are already separated because, as shown in Figs. 2(b)-(c), the L1-passing equi-potential curves, $F(x, y, 0) = J_{L1}$ and $F(x, 0, z) = J_{L1}$, do not turn back to go across the x -axis. Thus, the L2-passing equi-potential surfaces become the ones to form Roche Lobes.

Comparing Fig. 2(b) with Fig. 1(b), it is realized that there must be a transition with a critical mass M_g such that $J_{L1} = J_{L2}$, i.e. $F(x_{L1}, y_{L1}, z_{L1}) = F(x_{L2}, y_{L2}, z_{L2})$. In order to search for this critical value of M_g for any given m, R , we define a function

$$\begin{aligned} T_1(m, R, M_g) &\equiv F(x_{L1}, y_{L1}, z_{L1}) - F(x_{L2}, y_{L2}, z_{L2}) \\ &= F(0, 0, 0) - F(x_{L2}, 0, 0) \\ &= \frac{4m}{R} - n^2 x_{L2}^2 - \frac{2m}{x_{L2} + R} - \frac{2m}{x_{L2} - R} + \frac{4M_g}{\pi} \left(1 - \frac{\tan^{-1} x_{L2}}{x_{L2}} \right). \end{aligned} \quad (12)$$

If there is a zero point of function T_1 for a set of parameters m, R and M_g , this transition exists. From Eq.(12), the critical mass, denoted as M_1 , can be expressed as Eq. (13):

$$M_1 = \frac{\pi \left[n^2 x_{L2}^2 + \frac{2m}{x_{L2} + R} + \frac{2m}{x_{L2} - R} - \frac{4m}{R} \right]}{4 \left(1 - \frac{\tan^{-1} x_{L2}}{x_{L2}} \right)}. \quad (13)$$

We numerically solve M_1 as a function of R for different values of m , as presented in Fig. 5(a). For the case with $m = R = 1$, we find that $M_1 \sim 2.11$. If the critical mass M_1 exists, whether the total galactic mass M_g is larger than M_1 would determine the topology of the Roche Lobes. When $M_g < M_1$, two Roche Lobes are connected as the case shown in Fig. 1. When $M_g > M_1$, two Roche Lobes would be separated as shown in Figs. 2 and 3.

The difference between Figs.2 and 3 is whether or not there are Jiang-Yeh Points. There is a critical mass M_c to determine the existence of Jiang-Yeh point (Jiang & Yeh 2014a) and $M_c \sim 17.51$ when $m = R = 1$. Two Roche Lobes are separated in both plots due to $M_g > M_1$ for both Figs. 2 and 3. In Fig. 3, $M_g > M_c$, so there are Jiang-Yeh Points, and thus a Jiang-Yeh Lobe exists and is located between the separated Roche Lobes.

When $m = 1$ and $R = 2$, we find that $T_1(1, 2, M_g) > 0$ for any positive M_g . In this case, there is no zero point of T_1 and thus no critical mass M_1 . When no critical mass M_1 can be found, there is no such transition here.

On the other hand, it is shown that Roche Lobes are disconnected from the Jiang-Yeh Lobe in Fig. 3, but connected with the Jiang-Yeh Lobe in Fig. 4. Comparing Fig. 4(b) with Fig. 3(b), there must be a transition with a critical set of m , R and M_g so that $J_{JY1} = J_{L2}$, i.e. $F(x_{JY1}, y_{JY1}, z_{JY1}) = F(x_{L2}, y_{L2}, z_{L2})$. In order to search the critical set of m , R and M_g , we define a function :

$$\begin{aligned}
 T_2(m, R, M_g) &\equiv F(x_{JY1}, y_{JY1}, z_{JY1}) - F(x_{L2}, y_{L2}, z_{L2}) \\
 &= F(x_{JY1}, 0, 0) - F(x_{L2}, 0, 0) \\
 &= n^2(x_{JY1}^2 - x_{L2}^2) + 2m \left[\frac{1}{R - x_{JY1}} + \frac{1}{R + x_{JY1}} - \frac{1}{x_{L2} - R} - \frac{1}{x_{L2} + R} \right] \\
 &+ \frac{4M_g}{\pi} \left(\frac{\tan^{-1} x_{JY1}}{x_{JY1}} - \frac{\tan^{-1} x_{L2}}{x_{L2}} \right). \tag{14}
 \end{aligned}$$

A zero point of T_2 would correspond to a critical set of m , R , and M_g . When $T_2(m, R, M_g) = 0$, we find that M_g can be explicitly expressed as a function of m, R . We define this critical M_g to be M_2 :

$$M_2 = \frac{\pi \left[n^2(x_{L2}^2 - x_{JY1}^2) + \frac{2m}{x_{L2}+R} + \frac{2m}{x_{L2}-R} - \frac{2m}{R-x_{JY1}} - \frac{2m}{R+x_{JY1}} \right]}{4 \left(\frac{\tan^{-1} x_{JY1}}{x_{JY1}} - \frac{\tan^{-1} x_{L2}}{x_{L2}} \right)}. \tag{15}$$

From Eq. (15), we numerically solve M_2 as a function of R for different values of m , as shown in Fig. 5(b). It is found that M_2 is a decreasing function of the radius R for different values of m . When $m = R = 1$ and $M_g = 30$, the critical mass M_2 is huge, so $M_g < M_2$. When $m = 1, R = 2, M_g = 30$, the critical mass M_2 is less than 20, so $M_g > M_2$. Therefore, the results in Figs.3 and 4 are on different sides of this transition.

4. Mathematical Properties of the Jacobi Surfaces

Mathematical properties of the Jacobi surfaces, i.e. $F(x, y, z)$, are investigated in this section. From Eq.(11), partial derivatives of the function $F(x, y, z)$ can be calculated as:

$$\frac{\partial F}{\partial x} = 2n^2x - \frac{2m(x+R)}{r_1^3} - \frac{2m(x-R)}{r_2^3} + \frac{2cx}{r} \left\{ \frac{1}{(1+r^2)r} - \frac{\tan^{-1} r}{r^2} \right\} \tag{16}$$

$$\frac{\partial F}{\partial y} = 2y \left\{ n^2 - \frac{m}{r_1^3} - \frac{m}{r_2^3} + \frac{c}{r} \left[\frac{1}{(1+r^2)r} - \frac{\tan^{-1} r}{r^2} \right] \right\} \tag{17}$$

$$\frac{\partial F}{\partial z} = 2z \left\{ -\frac{m}{r_1^3} - \frac{m}{r_2^3} + \frac{c}{r} \left[\frac{1}{(1+r^2)r} - \frac{\tan^{-1} r}{r^2} \right] \right\}. \tag{18}$$

From Eq.(16), for convenience, we define :

$$\frac{\partial F}{\partial x} \Big|_{(x,y,z)=(x,0,0)} \equiv A(x). \quad (19)$$

Compared with the equations in Jiang & Yeh (2014a), we realize that the zero points of $A(x)$ are the equilibrium points on the x -axis. Moreover, as shown in Jiang & Yeh (2014a), there is a critical mass M_c which determines whether or not there are Jiang-Yeh Points. That is, there are JY1 and JY2 equilibrium points in the system if, and only if, $M_g > M_c$.

Property 1:

On the x -axis with $x_{L1} = 0 \leq x \leq x_{L2}$,

(a) when $M_g < M_c$, the maximum of $F(x, 0, 0)$ is at the location of the black hole $(R, 0, 0)$, and two relative minimum values of $F(x, 0, 0)$ are at 0 and x_{L2} ;

(b) when $M_g > M_c$, the maximum of $F(x, 0, 0)$ is at the location of the black hole $(R, 0, 0)$, and two relative minimum values of $F(x, 0, 0)$ are at x_{JY1} and x_{L2} .

(Proof):

According to Eq. (16), the equilibrium points of the system are zero points of $A(x)$. We first consider the function $F(x, 0, 0)$ in the interval (R, x_{L2}) , then in the interval (x_{L1}, R) (where $x_{L1}=0$) when $M_g < M_c$, and finally in the interval (x_{JY1}, R) when $M_g > M_c$.

(1) In the interval (R, x_{L2}) :

Since there is one equilibrium point L2 at $(x_{L2}, 0, 0)$ and no equilibrium point in (R, x_{L2}) , we have $A(x_{L2}) = 0$ and $A(x) \neq 0$ for $R < x < x_{L2}$. From Eq. (16), we find $\lim_{x \rightarrow R^+} A(x) = -\infty$, so $A(x) < 0$ for $R < x < x_{L2}$. From the definition of $A(x)$ in Eq. (19), $F(x, 0, 0)$ is a decreasing function in (R, x_{L2}) .

(2) In the interval (x_{L1}, R) with $M_g < M_c$:

The equilibrium point L1 is at $(0, 0, 0)$, so $x_{L1} = 0$ and $A(0) = 0$. In this case with $M_g < M_c$, there is no equilibrium point in $(0, R)$; thus, $A(x) \neq 0$ for $0 < x < R$. From Eq. (16), we find $A(R^-) = \infty$, which leads to $A(x) > 0$ for $0 < x < R$. Therefore, $F(x, 0, 0)$ is an increasing function in $(0, R)$.

(3) In the interval (x_{JY1}, R) with $M_g > M_c$:

When $M_g > M_c$, there is an equilibrium point JY1 in $(0, R)$, so $A(x_{JY1}) = 0$. There is no equilibrium point in (x_{JY1}, R) ; thus, $A(x) \neq 0$ for $x_{JY1} < x < R$. From Eq. (16), we find $A(R^-) = \infty$, which gives $A(x) > 0$ for $x_{JY1} < x < R$. That is, $F(x, 0, 0)$ is an increasing function in (x_{JY1}, R) .

The combination of (1) and (2) leads to that, for the interval $(0, x_{L2})$ on x -axis, $F(x, 0, 0)$ has the maximum value at $(R, 0, 0)$ and has local minimum values at $(0, 0, 0)$

and $(x_{L2}, 0, 0)$ when $M_g < M_c$. Thus, **(a)** is proved.

The combination of **(1)** and **(3)** leads to that, for the interval (x_{JY1}, x_{L2}) on x -axis, $F(x, 0, 0)$ has the maximum value at $(R, 0, 0)$ and has local minimum values at $(x_{JY1}, 0, 0)$ and $(x_{L2}, 0, 0)$ when $M_g > M_c$. Thus, **(b)** is proved. \square

Property 2:

(a) Along the line $x = R$ of the xy -plane, the maximum value of $F(R, y, 0)$ is at the black hole $(R, 0, 0)$, and there is a relative minimum of $F(R, y, 0)$ at a point $y^* > 0$.

(b) Along the line $x = R$ of the xz -plane, the maximum value of $F(R, 0, z)$ is at the black hole $(R, 0, 0)$.

(Proof):

(a) From Eq.(17), we define

$$\begin{aligned} B_R(y) &= \left. \frac{\partial F}{\partial y} \right|_{(x,y,z)=(R,y,0)} = 2y \left\{ n^2 - \frac{m}{r_1^3} - \frac{m}{r_2^3} + \frac{c}{r} \left[\frac{1}{(1+r^2)r} - \frac{\tan^{-1} r}{r^2} \right] \right\} \\ &\equiv 2y [-P(y) + Q(y)], \end{aligned} \quad (20)$$

where $P(y) = \frac{m}{r_1^3} + \frac{m}{r_2^3} - n^2$, $Q(y) = \frac{c}{r} \left[\frac{1}{(1+r^2)r} - \frac{\tan^{-1} r}{r^2} \right]$, $r_1^2 = 4R^2 + y^2$, $r_2^2 = y^2$, and $r^2 = R^2 + y^2$. For positive y , since $\lim_{y \rightarrow 0} yP(y) = \infty$ and $\lim_{y \rightarrow 0} yQ(y) = 0$, we know $\lim_{y \rightarrow 0} B_R(y) = -\infty$. Moreover, because $\lim_{y \rightarrow \infty} yP(y) = -\infty$ and $\lim_{y \rightarrow \infty} yQ(y) = 0$, we have $\lim_{y \rightarrow \infty} B_R(y) = \infty$. Thus, there is at least one point in the interval $(0, \infty)$, such that $B_R(y) = 0$. We assume the smallest zero point to be $y^* \in (0, \infty)$ such that $B_R(y^*) = 0$. Since $B_R(y) = \left. \frac{\partial F}{\partial y} \right|_{(R,y,0)} < 0$ for $0 < y < y^*$, there is a relative minimum of $F(R, y, 0)$ at point $y^* > 0$.

Because $B_R(-y) = -B_R(y)$, we can similarly have a zero point $y_1^* \in (-\infty, 0)$ such that $B_R(y_1^*) = 0$. Since $B_R(y) = \left. \frac{\partial F}{\partial y} \right|_{(R,y,0)} < 0$ for $0 < y < y^*$ and $B_R(y) = \left. \frac{\partial F}{\partial y} \right|_{(R,y,0)} > 0$ for $y_1^* < y < 0$, there is a maximum value of $F(R, y, 0)$ at the black hole $(R, 0, 0)$ along the y -axis.

(b) From Eqs.(18) and (8), we have :

$$\left. \frac{\partial F}{\partial z} \right|_{(x,y,z)=(R,0,z)} = 2z \left\{ -\frac{m}{r_1^3} - \frac{m}{r_2^3} + \frac{c}{r} \left[\frac{1}{(1+r^2)r} - \frac{\tan^{-1} r}{r^2} \right] \right\} = 2z \left\{ -\frac{m}{r_1^3} - \frac{m}{r_2^3} + \frac{f_g(r)}{r} \right\},$$

where $r_1^2 = 4R^2 + z^2$, $r_2 = |z|$, $r^2 = R^2 + z^2$. Because the gravitational force $f_g(r) < 0$ at any r , $\left. \frac{\partial F}{\partial z} \right|_{(R,0,z)} < 0$ for $z > 0$ and $\left. \frac{\partial F}{\partial z} \right|_{(R,0,z)} > 0$ for $z < 0$, there is a maximum value of $F(R, 0, z)$ at the black hole $(R, 0, 0)$ along the z -axis. \square

Property 3:

(a) Along the y -axis of the xy -plane, the maximum value of $F(0, y, 0)$ is at the origin $(0, 0, 0)$. In addition, there is one relative minimum value of $F(0, y, 0)$ at y_{L4} , and another relative minimum value of $F(0, y, 0)$ at y_{L5} .

(b) When $M_g > M_c$, we have $0 < z_d < y_d < x_{JY1}$; z_d and y_d are defined in Section 3.

(c) Along the z -axis of xz -plane, the maximum value of $F(0, 0, z)$ is at the origin $(0, 0, 0)$.

(Proof):

(a) From Eq.(17), for $y > 0$, we define :

$$\begin{aligned} B_0(y) &= \left. \frac{\partial F}{\partial y} \right|_{(x,y,z)=(0,y,0)} = 2y \left\{ n^2 - \frac{m}{r_1^3} - \frac{m}{r_2^3} + \frac{c}{y} \left[\frac{1}{(1+y^2)y} - \frac{\tan^{-1} y}{y^2} \right] \right\} \\ &\equiv 2y [-P(y) + Q(y)], \end{aligned} \quad (21)$$

where $P(y) = \frac{m}{r_1^3} + \frac{m}{r_2^3} - n^2$, $Q(y) = c \left[\frac{1}{(1+y^2)y^2} - \frac{\tan^{-1} y}{y^3} \right]$, and $r_1^2 = r_2^2 = R^2 + y^2$. From the above definition of $Q(y)$, we have :

$$\lim_{y \rightarrow 0} Q(y) = \lim_{y \rightarrow 0} \frac{c}{y^3} \left(\frac{y}{1+y^2} - \tan^{-1} y \right) = \lim_{y \rightarrow 0} \frac{-2cy^2}{3y^2(1+y^2)^2} = -\frac{2c}{3} < 0, \quad (22)$$

and

$$Q'(y) = c \frac{-3y - 5y^3 + 3(1+y^2)^2 \tan^{-1}(y)}{y^4(1+y^2)^2} = c \left\{ \frac{3(1+y^2)^2 g_1(y)}{y^4(1+y^2)^2} \right\}, \quad (23)$$

where $g_1(y) \equiv \tan^{-1} y - \frac{5y^3+3y}{3(1+y^2)^2}$. Since $g_1'(y) = \frac{8y^4}{3(1+y^2)^3} > 0$ for $y > 0$ and $g_1(0) = 0$, we have $g_1(y) > 0$ for $y > 0$. Thus, from Eq. (23), we know $Q'(y) > 0$ for all $y > 0$. Therefore, from Eqs.(22) and (23), we have $-\frac{2c}{3} < Q(y) < 0$ for $y > 0$. Moreover, from Eqs.(22) and (9), we have :

$$\lim_{y \rightarrow 0} [-P(y) + Q(y)] = -\frac{2m}{R^3} + n^2 - \frac{2c}{3} = -\frac{7m}{4R^3} + \left[|Q(R)| - \frac{2c}{3} \right] < 0, \quad (24)$$

so $\lim_{y \rightarrow 0} B_0(y) = \lim_{y \rightarrow 0} 2y[-P(y) + Q(y)] = 0$. Since $B_0'(y) = 2[-P(y) + Q(y)] + 2y[-P'(y) + Q'(y)]$, from Eq.(24), we have $B_0'(0) = 2[-P(0) + Q(0)] < 0$. According to Eq.(17), the equilibrium points of the system are zero points of $B_0(y)$. Since there is one equilibrium point L4 at $(0, y_{L4}, 0)$ and no equilibrium point in $y \in (0, y_{L4})$, we have $B_0(0) = B_0(y_{L4}) = 0$, $B_0(y) \neq 0$ for $0 < y < y_{L4}$ and $B_0'(0) < 0$. Therefore, $B_0(y) = \left. \frac{\partial F}{\partial y} \right|_{(x,y,z)=(0,y,0)} < 0$ for $0 < y < y_{L4}$; there is a relative minimum value of $F(0, y, 0)$ at point y_{L4} .

Through a similar method, it can be shown that $\left. \frac{\partial F}{\partial y} \right|_{(x,y,z)=(0,y,0)} > 0$ for $y_{L5} < y < 0$, and there is a relative minimum value of $F(0, y, 0)$ at point y_{L5} . Therefore, along the y -axis of xy -plane, the maximum value of $F(0, y, 0)$ is at the origin $(0, 0, 0)$.

(b) When $M_g > M_c$, JY1 exists. As $F(x_{JY1}, 0, 0)$ is the value of Jacobi integral at JY1, we set $F(x_{JY1}, 0, 0) = J_{JY1}$. Thus, $F(x, y, 0) = J_{JY1}$ is the JY1-passing equi-potential curve on xy -plane. Since $(0, y_d, 0)$ is the intersection between $F(x, y, 0) = J_{JY1}$ and y -axis, y_d is the root of $F(0, y, 0) = J_{JY1}$. To examine the existence of y_d , we define :

$$k_y(y) \equiv F(0, y, 0) - F(x_{JY1}, 0, 0) = n^2(y^2 - x_{JY1}^2) + 2m \left(\frac{2}{\sqrt{R^2 + y^2}} - \frac{1}{R + x_{JY1}} - \frac{1}{R - x_{JY1}} \right) + 2c \left[\frac{\tan^{-1}|y|}{|y|} - \frac{\tan^{-1} x_{JY1}}{x_{JY1}} \right]. \quad (25)$$

From Fig. 6, we find that $k_y(0) > 0$ for considered values of m , R , and M_g . From Eq.(25), we have :

$$k_y(x_{JY1}) = 2m \left(\frac{2}{\sqrt{R^2 + x_{JY1}^2}} - \frac{1}{R + x_{JY1}} - \frac{1}{R - x_{JY1}} \right) = 2m \left(\frac{2(R^2 - x_{JY1}^2) - 2R\sqrt{R^2 + x_{JY1}^2}}{\sqrt{R^2 + x_{JY1}^2}(R + x_{JY1})(R - x_{JY1})} \right) = 4m \left(\frac{R(R - \sqrt{R^2 + x_{JY1}^2}) - x_{JY1}^2}{\sqrt{R^2 + x_{JY1}^2}(R + x_{JY1})(R - x_{JY1})} \right) < 0.$$

Thus, there is a point $y_d \in (0, x_{JY1})$ such that $k_y(y_d) = 0$.

Further, we define :

$$k_z(z) = F(0, 0, z) - F(x_{JY1}, 0, 0) = -n^2 x_{JY1}^2 + 2m \left(\frac{2}{\sqrt{R^2 + z^2}} - \frac{1}{R + x_{JY1}} - \frac{1}{R - x_{JY1}} \right) + 2c \left[\frac{\tan^{-1}|z|}{|z|} - \frac{\tan^{-1} x_{JY1}}{x_{JY1}} \right]. \quad (26)$$

From Eqs.(25)-(26), we have $k_z(0) = k_y(0) > 0$. In addition, we also have :

$$k_z(y_d) = -n^2 x_{JY1}^2 + 2m \left(\frac{2}{\sqrt{R^2 + y_d^2}} - \frac{1}{R + x_{JY1}} - \frac{1}{R - x_{JY1}} \right) + 2c \left[\frac{\tan^{-1} y_d}{y_d} - \frac{\tan^{-1} x_{JY1}}{x_{JY1}} \right] = k_y(y_d) - n^2 y_d^2.$$

Because $k_y(y_d) = 0$, we have $k_z(y_d) = -n^2 y_d^2 < 0$. Thus, there is a point $z_d \in (0, y_d)$ such that $k_z(z_d) = 0$. Therefore, we have $0 < z_d < y_d < x_{JY1}$.

(c) From Eqs.(18) and (8), we have

$$\frac{\partial F}{\partial z} \Big|_{(x,y,z)=(0,0,z)} = 2z \left\{ -\frac{m}{r_1^3} - \frac{m}{r_2^3} + \frac{c}{r} \left[\frac{1}{(1+r^2)r} - \frac{\tan^{-1} r}{r^2} \right] \right\} = 2z \left\{ -\frac{m}{r_1^3} - \frac{m}{r_2^3} + \frac{f_g(r)}{r} \right\},$$

where $r_1^2 = r_2^2 = R^2 + z^2$, $r = |z|$. Since the gravitational force $f_g(r) < 0$, we have $\frac{\partial F}{\partial z} < 0$ for $z > 0$ and $\frac{\partial F}{\partial z} > 0$ for $z < 0$. Therefore, along the z -axis, there is a maximum value of $F(0, 0, z)$ at the origin $(0, 0, 0)$. \square

5. The Determination of Lobe Regions

In order to know whether a particle is inside the Roche Lobes or Jiang-Yeh Lobe, we need a standard procedure to determine the regions of lobes. One possibility is to numerically determine the Roche Lobes or Jiang-Yeh Lobe and keep the coordinates of these surfaces. To judge whether a particle is inside these closed surfaces, we can simply compare the particle's coordinate with the coordinate of this particle's corresponding point projected onto these surface along one of the axes of coordinate system. However, one would need to do a multi-dimensional numerical interpretation to get this projection done. When particles are very close to one of these surfaces, one would need much higher resolution on the numerical coordinates of surfaces, so it would be a very time-consuming process.

In order to avoid this difficult, we propose another procedure which is based on the monotonic behavior of the Jacobi integral of equi-potential surfaces. After the coordinates of equilibrium points and other important points are found, the smallest radius, r_R , of the shell which can enclose the Roche Lobe centered on $(R, 0, 0)$ can be determined. Similarly, the smallest radius, r_{JY} , of the shell enclosing the Jiang-Yeh Lobe centered on $(0, 0, 0)$ can be determined, too. For example, in Model A, r_R is set as the largest among $|x_a - R|$, $|R - x_{L1}|$, y_a , z_a , so it is the smallest radius which can enclose the Roche Lobe. Similarly, for Model B, r_R is the largest among $|x_b - R|$, $|R - x_{L2}|$, y_b , z_b . For Model C, the smallest radius r_R that can enclose Roche Lobe is defined in the same way as in Model B; and the smallest radius r_{JY} that can enclose Jiang-Yeh Lobe is defined as the largest among x_{JY1} , y_d and z_d . For Model D, the smallest radius r_R that can enclose Roche Lobe is the largest among $|x_c - R|$, $|R - x_{JY1}|$, y_c , z_c ; and the smallest radius r_{JY} that can enclose Jiang-Yeh Lobe is determined in the same way as in Model C. After r_R and r_{JY} are determined, we then need to confirm that the Jacobi integral of equi-potential surfaces is either monotonically decreasing or monotonically increasing from the centers of the lobes. Through the comparisons between the values of Jacobi integrals of equi-potential surfaces at a particle's coordinate and at the boundary of a particular lobe, we can know whether this particle is in the lobe region. The exact steps are listed as follows:

Step 1. Determine the locations of equilibrium points numerically i.e. $(x_{L1}, y_{L1}, 0)$, $(x_{L2}, y_{L2}, 0)$, $(x_{L3}, y_{L3}, 0)$, $(x_{L4}, y_{L4}, 0)$, $(x_{L5}, y_{L5}, 0)$, $(x_{JY1}, y_{JY1}, 0)$, $(x_{JY2}, y_{JY2}, 0)$. Please note that $x_{L1} = y_{L1} = y_{L2} = y_{L3} = x_{L4} = x_{L5} = y_{JY1} = y_{JY2} = 0$.

Step 2. Draw zero-velocity curves which pass through L1, L2 and JY1 on xy -plane and yz -plane. Then, numerically determine the intersection points between these curves and coordinate axes, and also the intersection points between these curves and straight lines which go through the lobe center and are parallel with x -axis, y -axis, or z -axis. For example,

those marked points $x_a, x_b, y_b...$ etc. in Figs. 1-4.

Step 3. Determine the smallest radius of shells which can enclose the lobes, i.e. r_R and r_{JY} .

Step 4. Numerically show that $F(x, y, z)$ is monotonically decreasing or increasing from the center to the boundaries of these shells. If $\frac{\partial F}{\partial x} < 0$, $\frac{\partial F}{\partial y} < 0$, and $\frac{\partial F}{\partial z} < 0$ inside shells, $F(x, y, z)$ is monotonically decreasing from the centers to the boundaries. When $\frac{\partial F}{\partial x} > 0$, $\frac{\partial F}{\partial y} > 0$, and $\frac{\partial F}{\partial z} > 0$ inside shells, then $F(x, y, z)$ is monotonically increasing from the centers to the boundaries.

Step 5. Compare the values of $F(x, y, z)$. For a particle with coordinates (x_p, y_p, z_p) , we first determine whether it is inside one of the shells that enclose Roche Lobes or Jiang-Yeh Lobe. If it is inside the shell enclosing one of the Roche Lobes, we use the value $F(x_p, y_p, z_p)$ to judge whether it is inside or outside of the Roche Lobe by comparing its value with $F(x_{L1}, y_{L1}, 0)$ when two Roche Lobes are connected (as the case in Model A), and by comparing its value with $F(x_{L2}, y_{L2}, 0)$ when two Roche Lobes are separated (as the case in Model B). If it is inside the shell enclosing Jiang-Yeh Lobe, we use the value $F(x_p, y_p, z_p)$ to judge whether it is inside or outside of the Jiang-Yeh Lobe by comparing its value with $F(x_{JY1}, y_{JY1}, 0)$.

Therefore, through the above five steps, whether a particle is inside one of lobe regions can be determined completely by numerical calculations. In the case that some mathematical properties of the system are studied analytically, the known analytical results, as those presented in previous section, can be used to reconfirm parts of numerical calculations in Steps 3 and 4. The numerical values of coordinates of those important points in Model A-D are presented in Table 1. These values determined by numerical calculations completely satisfy the mathematical properties we have proven.

6. Concluding Remarks

We have studied a galactic model with supermassive binary holes. Assuming two black holes have equal mass, the three-dimensional equi-potential surfaces, i.e. Roche Lobes and Jiang-Yeh Lobe are presented. The critical conditions of two kinds of topological transitions for these equi-potential surfaces were investigated herein. When the galactic total mass $M_g = 0$, two Roche Lobes are connected at the first Lagrange Point. When M_g is larger, in one case, two Roche Lobes would separate first, and a detached Jiang-Yeh Lobe shows up in the middle for an even larger value of M_g ; in another case, the Jiang-Yeh Lobe appears directly and three lobes are connected. The mathematical properties of the Jacobi surfaces, $F(x, y, z)$, are also investigated. In addition, a numerical procedure to determine the regions of Roche Lobes and Jiang-Yeh Lobe is described herein.

The main limitation of our model is that two supermassive black holes are assumed to have equal mass and move in a circular orbit. Thus, our model might not be used to study the galactic minor mergers, but could be a good approximation to investigate the process of galactic major mergers. In a galactic major merger, both involved systems would have similar configurations. Due to the dynamical friction, both supermassive black holes in galaxies migrate into the central region until most surrounding stars are scattered out and the dynamical friction becomes very small. These two supermassive black holes will form an equal mass binary system and move in a circular orbit. This is the stage during the galactic evolution that our model can act as a good tool to investigate the distribution and kinematics of stars in the system. Therefore, our model can lead to a prediction of surface brightness and line-of-sight velocity distribution of the galactic systems which experienced major mergers. Future observations can test these predictions and the roles of Jiang-Yeh Lobe and Roche Lobes will be clear after comparisons between theoretical predictions and observational results are performed.

Acknowledgment

We are grateful to the referee for good suggestions. This work is supported in part by the Ministry of Science and Technology, Taiwan, under Li-Chin Yeh's Grants MOST 104-2115-M-134-004 and Ing-Guey Jiang's Grants MOST 103-2112-M-007-020-MY3.

REFERENCES

- Chermnykh, S. V., 1987, *Vest. Leningrad Univ.* 2, 10
- Douskos, C. N., 2011, *Astrophysics and Space Science*, 333, 79
- Douskos, C. N., 2015, *Astrophysics and Space Science*, 356, 251
- Douskos, C. N., Kalantonis, V., Markellos, P., Perdios, E., 2012, *Astrophysics and Space Science*, 337, 99
- Eggleton, P. P., 1983, *ApJ*, 268, 368
- Hernquist, L., 1990, *ApJ*, 356, 359
- Jiang, I.-G., Yeh, L.-C., 2006, *Astrophysics and Space Science*, 305, 341
- Jiang, I.-G., Yeh, L.-C., 2014a, *Astrophysics and Space Science*, 349, 881
- Jiang, I.-G., Yeh, L.-C., 2014b, *Astrophysics and Space Science*, 354, 525
- Kandrup, H. E., Sideris, I. V., Terzic, B. Bohn, C. L., 2003, *ApJ*, 597, 111
- Kishor, R., Kushvah, B. S., 2013, *Astrophysics and Space Science*, 344, 333
- Kushvah, B. S., 2008a, *Astrophysics and Space Science*, 315, 231
- Kushvah, B. S., 2008b, *Astrophysics and Space Science*, 318, 41
- Kushvah, B. S., 2009, *Astrophysics and Space Science*, 323, 57
- Kushvah, B. S., 2011a, *Astrophysics and Space Science*, 332, 99
- Kushvah, B. S., 2011b, *Astrophysics and Space Science*, 333, 49
- Kushvah, B. S., Kishor, R., Dolas, U., 2012, *Astrophysics and Space Science*, 337, 115
- Mikkola, S., Innanen, K. A., Muinonen, K., Bowell, E., 1994, *Celestial Mechanics and Dynamical Astronomy*, 58, 53
- Milosavljevic, M., Merritt, D., 2001, *ApJ*, 563, 34
- Namouni, F., 1999, *Icarus*, 137, 293
- Papadakis, K. E., 2004, *A&A*, 425, 1133
- Papadakis, K. E., 2005a, *Astrophysics and Space Science*, 299, 67

- Papadakis, K. E., 2005b, *Astrophysics and Space Science*, 299, 129
- Perdios, E. A., Kalantonis, V. S., Douskos, C. N., 2008, *Astrophysics and Space Science*, 314, 199
- Quinlan, G. D., 1996, *New Astronomy*, 1, 35
- Wu, Y.-T., Jiang, I.-G., 2009, *MNRAS*, 399, 628
- Wu, Y.-T., Jiang, I.-G., 2012, *ApJ*, 745, 105
- Wu, Y.-T., Jiang, I.-G., 2015, *ApJ*, 805, 32
- Yeh, L.-C., Chen, Y.-C., Jiang, I.-G., 2012, *Int. J. Bifurcation and Chaos*, 22, 1230040
- Yeh, L.-C., Jiang, I.-G., 2006, *Astrophysics and Space Science*, 306, 189
- Zhao, H.S., 1996, *MNRAS*, 278, 488

Table 1

Model	A	B	C	D
M_g	0	10	30	30
m	1	1	1	1
R	1	1	1	2
x_{L1}	0.0	0.0	0.0	0.0
x_{L2}	2.3968	1.6989	1.5014	2.6753
x_{JY1}	–	–	0.3608	1.3646
x_a	1.810	–	–	–
x_b	–	0.4396	0.5932	–
x_c	–	–	–	2.5426
y_{L4}	1.7320	1.1517	1.0604	2.0318
y_a	0.7481	0.5596	–	–
y_b	0.9646	0.4727	0.3380	0.4463
y_c	–	–	0.3813	0.4275
y_d	–	–	0.1498	1.039
z_a	0.7123	0.4881	–	–
z_b	0.8732	0.4320	0.3091	0.4180
z_c	–	–	0.3382	0.4033
z_d	–	–	0.1165	0.8751
r_R	1	0.6989	0.5014	1.5426
r_{JY}	–	–	0.3608	1.3646

Table 1: The values of parameters, coordinates, and radii in Model A,B,C,D.

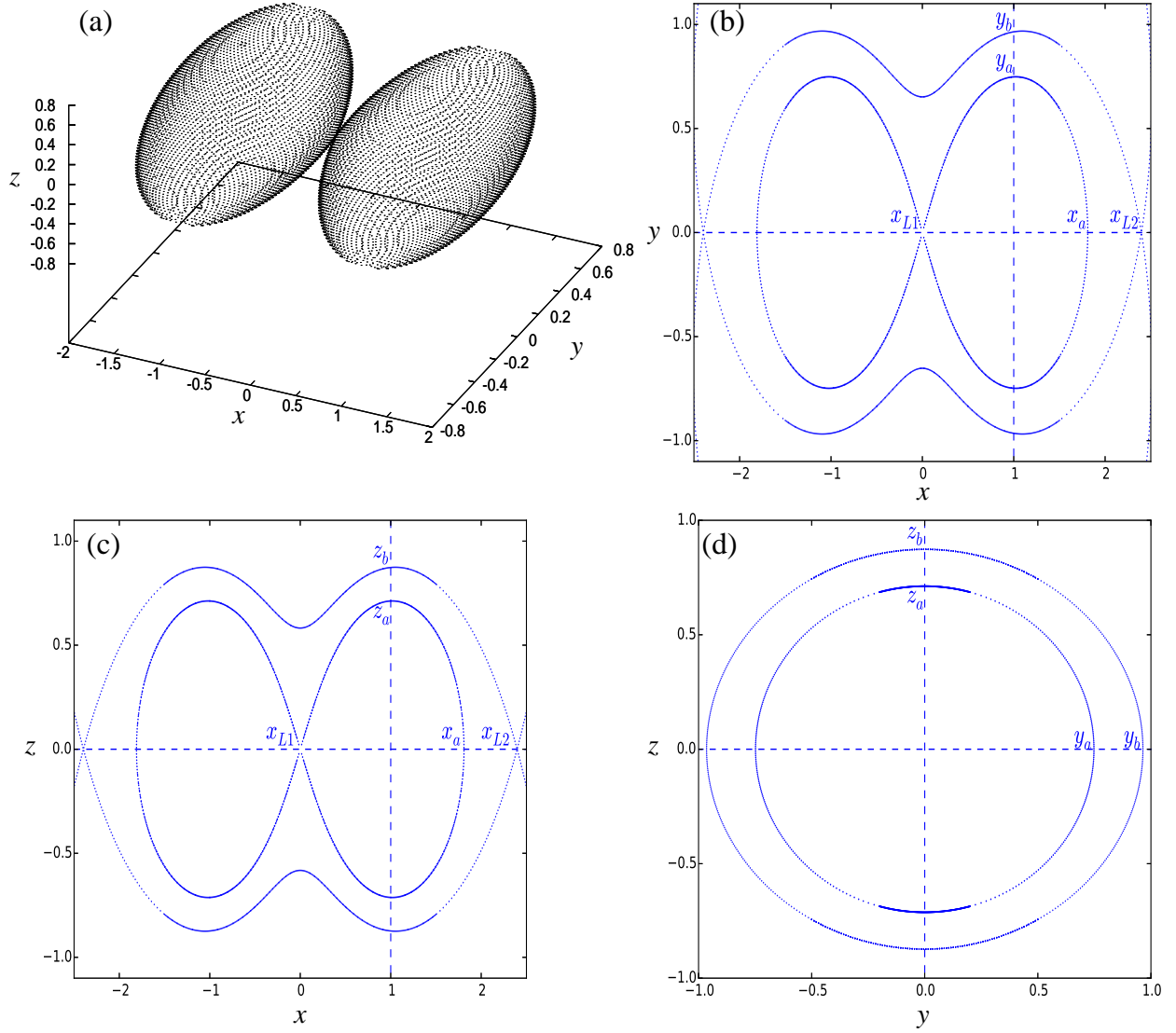


Fig. 1.— The Roche Lobes and equi-potential curves when $m = R = 1$ and $M_g = 0$ (Model A). (a) The Roche Lobes in three dimensional space. (b) The equi-potential curves on the xy -plane with $z = 0$. (c) The equi-potential curves on the xz -plane with $y = 0$. (d) The equi-potential curves on the yz -plane with $x = R$.

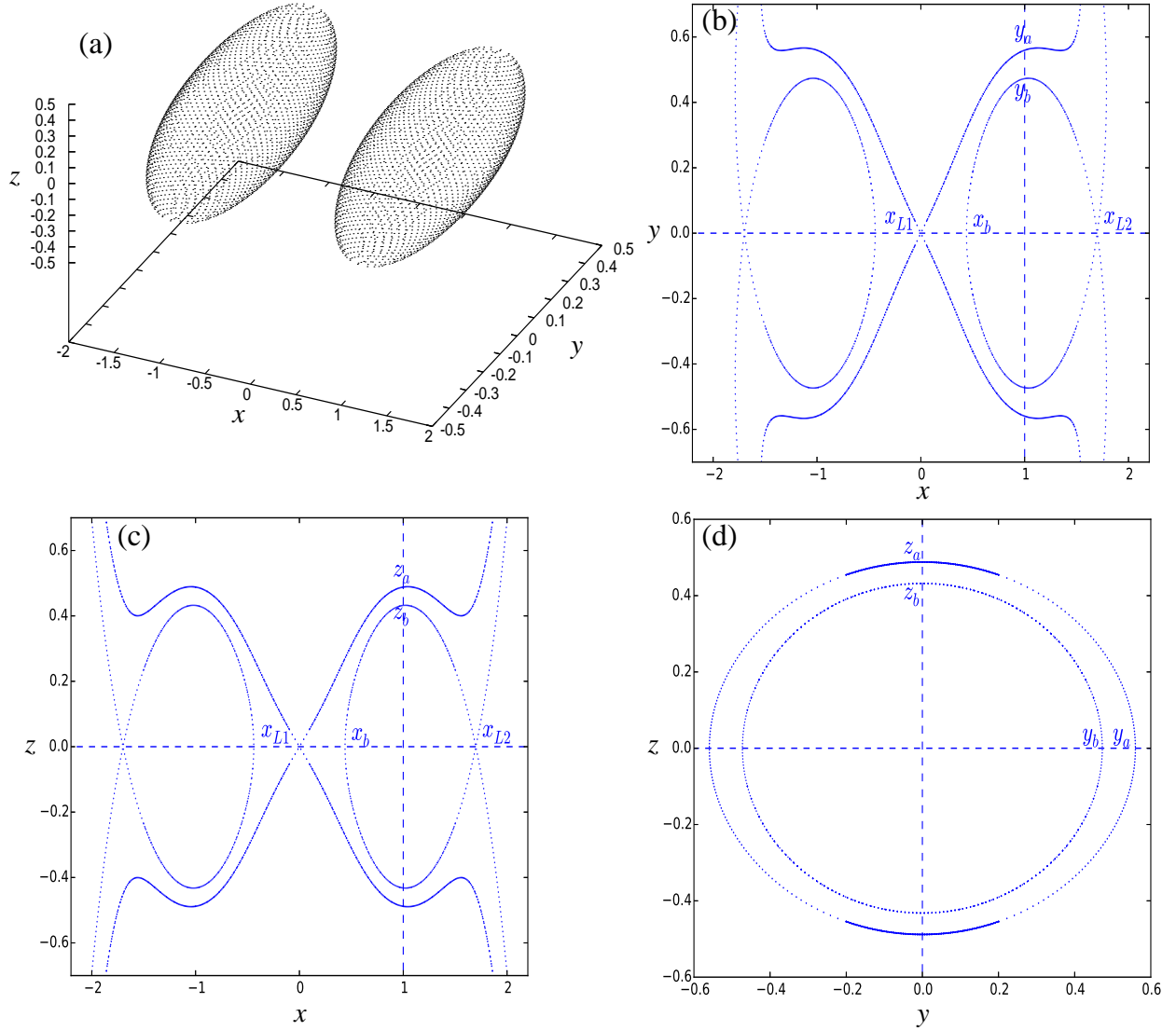


Fig. 2.— The Roche Lobes and equi-potential curves when $m = R = 1$ and $M_g = 10$ (Model B). (a) The Roche Lobes in three dimensional space. (b) The equi-potential curves on the xy -plane with $z = 0$. (c) The equi-potential curves on the xz -plane with $y = 0$. (d) The equi-potential curves on the yz -plane with $x = R$.

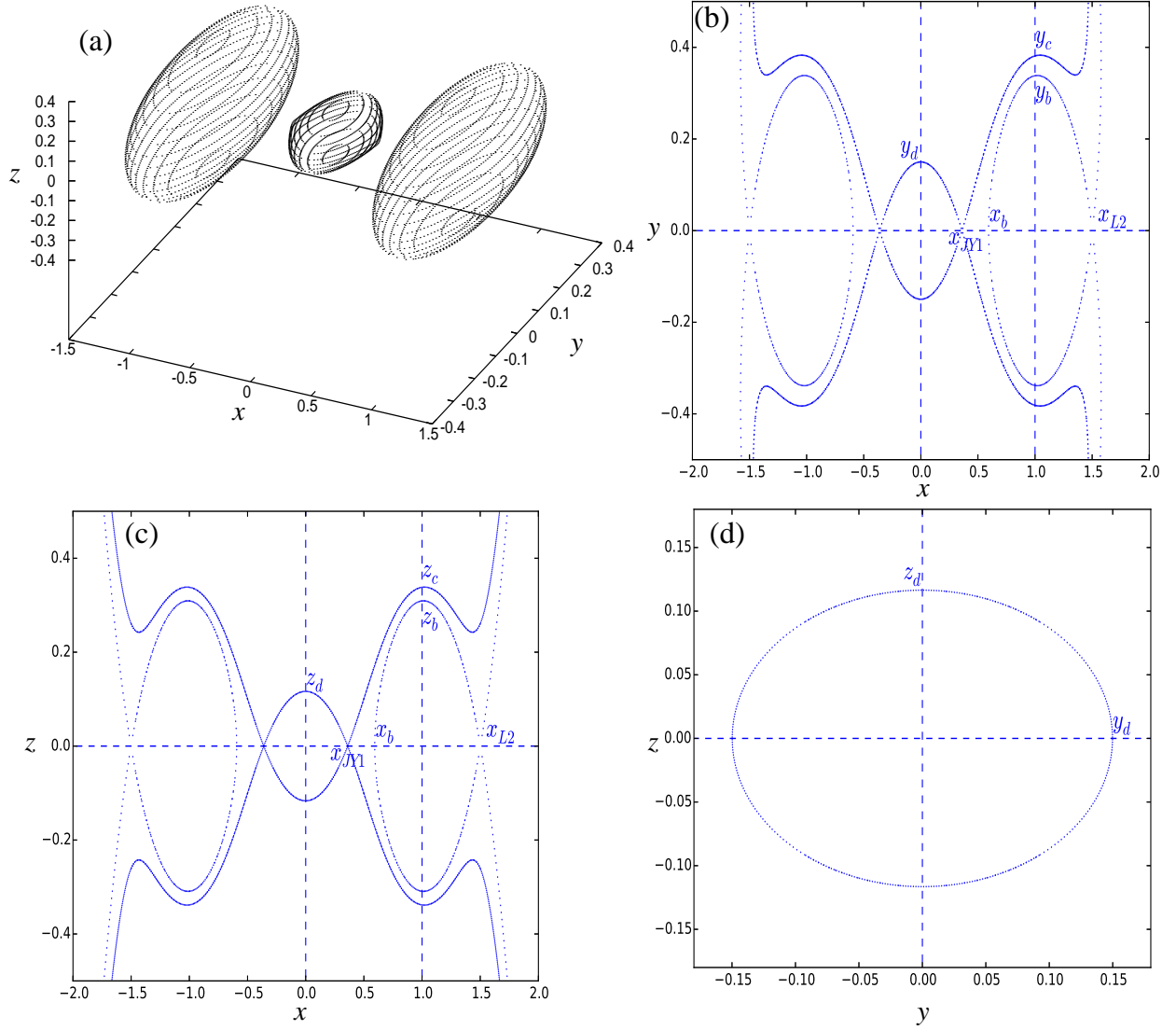


Fig. 3.— The Roche Lobes, Jiang-Yeh Lobe, and equi-potential curves when $m = R = 1$ and $M_g = 30$ (Model C). (a) The Roche Lobes and Jiang-Yeh Lobe in three dimensional space. (b) The equi-potential curves on the xy -plane $z = 0$. (c) The equi-potential curves on the xz -plane $y = 0$. (d) The equi-potential curves on the yz -plane with $x = 0$.

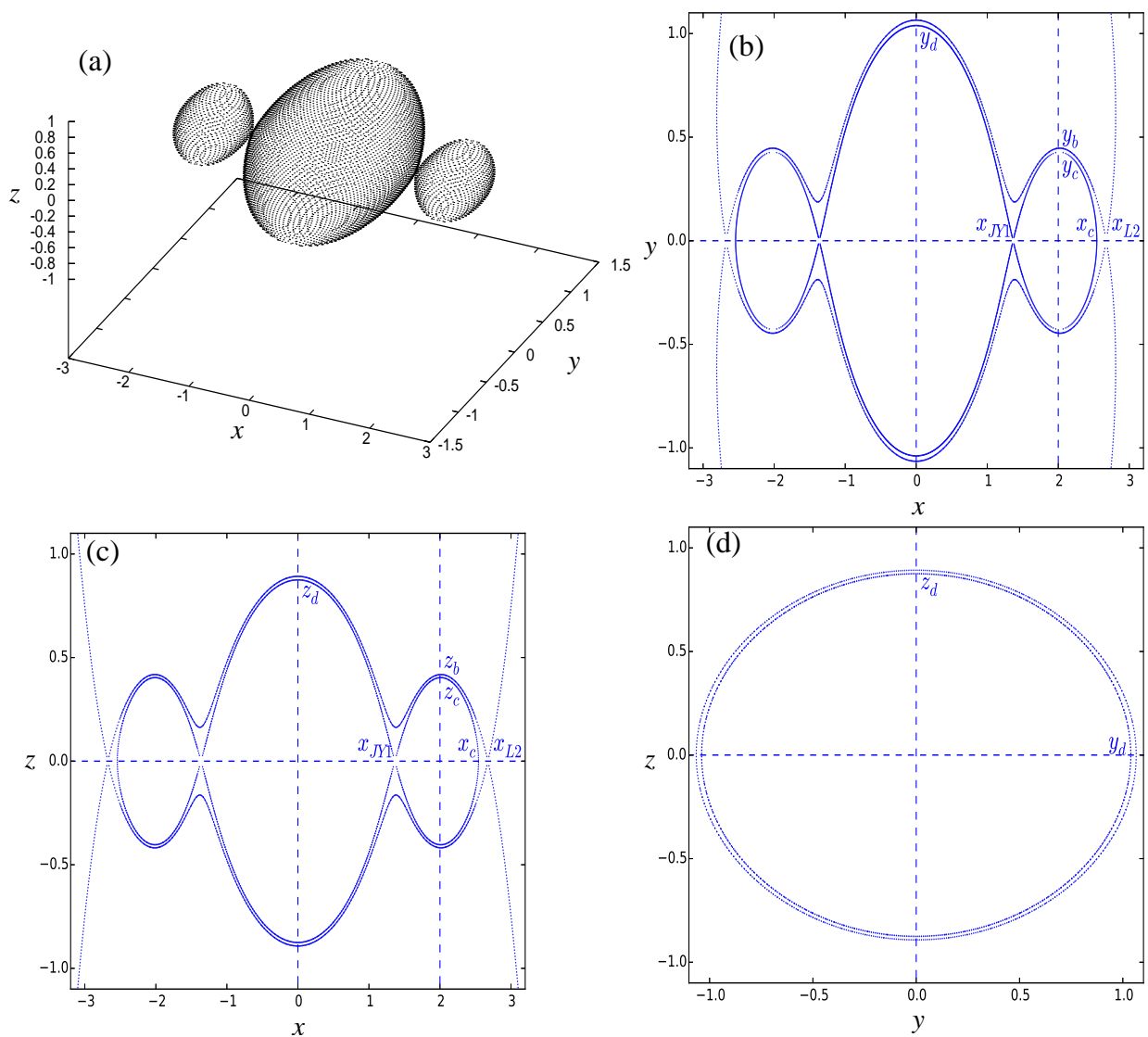


Fig. 4.— The Roche Lobes, Jiang-Yeh Lobe, and equipotential curves when $m = 1$, $R = 2$, and $M_g = 30$ (Model D). (a) The Roche Lobes and Jiang-Yeh Lobe in three dimensional space. (b) The equipotential curves on the xy -plane $z = 0$. (c) The equipotential curves on the xz -plane $y = 0$. (d) The equipotential curves on the yz -plane with $x = 0$.

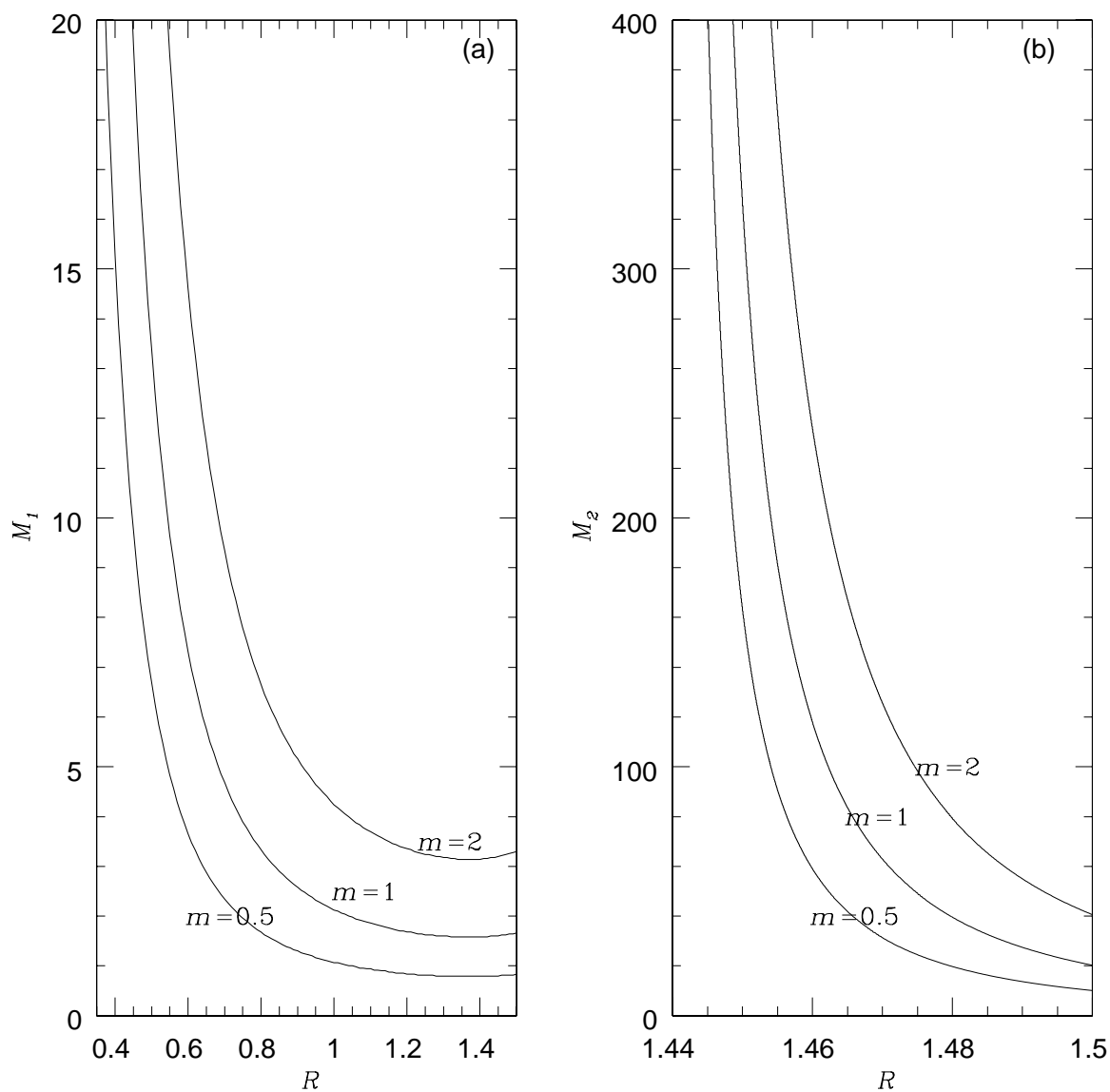


Fig. 5.— The critical masses of transitions. (a) M_1 as a function of R for different values of m . (b) M_2 as a function of R for different values of m .

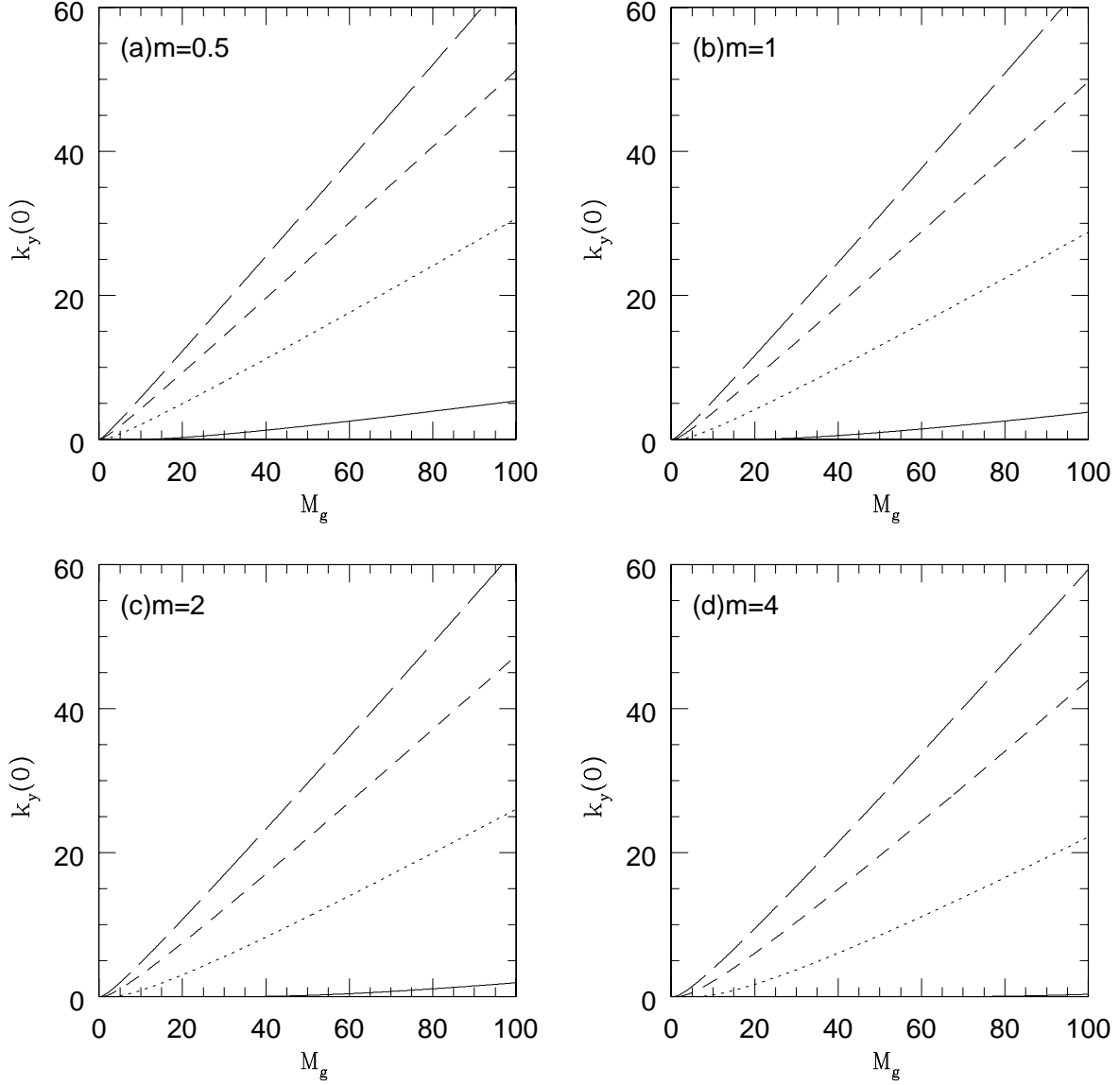


Fig. 6.— The values of $k_y(0)$ as a function of M_g for different values of m and R . (a) is for $m = 0.5$; (b) is for $m = 1$; (c) is for $m = 2$; (d) is for $m = 4$. In all panels, the solid line is for $R = 1$; the dotted line is for $R = 2$; the dashed line is for $R = 3$; and the long-dashed line is for $R = 4$.